JGR Space Physics

Key Points:

- 2-D global hybrid simulations are performed to study quasi-parallel magnetosheath high-speed jets (HSJs)
- The elongated HSJs formed at the quasi-parallel shock extend toward the quasi-perpendicular magnetosheath, and the traces of HSJs are filamentary structures
- The solar wind conditions and the convergence of several HSJs lead to the formation of a large-scale HSJ

Correspondence to:

S. Lu and Q. Lu,
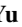lusan@ustc.edu.cn;
qmlu@ustc.edu.cn
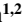
Large-Scale High-Speed Jets in Earth's Magnetosheath: Global Hybrid Simulations

Jin Guo[1,2] , **San Lu[1,2]** , **Quanming Lu[1,2]** , **Yu Lin[3]** , **Xueyi Wang[3]** , **Junyi Ren[1,2]**, **Yufei Hao[4]** , **Kai Huang[1,2]** , **Rongsheng Wang[1,2]** , and **Xinliang Gao[1,2]**

[1]CAS Key Lab of Geospace Environment, School of Earth and Space Sciences, University of Science and Technology of China, Hefei, China, [2]CAS Center for Excellence in Comparative Planetology, Hefei, China, [3]Physics Department, Auburn University, Auburn, AL, USA, [4]Key Laboratory of Planetary Sciences, Purple Mountain Observatory, Chinese Academy of Sciences, Nanjing, China

Abstract High-speed jets (HSJs) occur frequently in Earth's magnetosheath downstream of the quasiparallel bow shock. They have great impacts on the magnetosheath and the magnetosphere. Using two-dimensional global hybrid simulations, we investigate the formation and evolution of HSJs with different solar wind conditions. When the quasi-parallel shock is formed, HSJs begin to appear in the quasi-parallel magnetosheath. Some elongated HSJs formed at the quasi-parallel bow shock extend toward the quasi-perpendicular magnetosheath along with the background magnetosheath flow. As the elongated HSJs moves in the magnetosheath, filamentary structures of the velocity, ion density, and temperature occur in the magnetosheath. The filamentary structures are the traces of HSJs moving in the magnetosheath. Moreover, the Kelvin-Helmholtz instability can be excited at HSJs, which causes meandering of HSJs. When the interplanetary magnetic field is aligned to the solar wind velocity, the large-scale HSJs with a parallel (perpendicular) scale size of about 2.5 R_E (0.3 R_E) are formed at the magnetosheath where the θ_{Bn} is approaching zero. Then, some HSJs converge, leading to the formation of even larger HSJs with a parallel (perpendicular) scale size of 5 R_E (0.6 R_E).

1. Introduction

Collisionless shocks are ubiquitous in space plasmas. The Earth's bow shock acts to decelerate the solar wind from supermagnetosonic to submagnetosonic speeds (Fairfield, 1971; Peredo et al., 1995). Downstream of the bow shock is the magnetosheath, and the earthward boundary of the magnetosheath is the Earth's magnetopause. Plasma properties of the magnetosheath are highly dependent on the upstream interplanetary magnetic field (IMF) direction. When the angle between the shock normal direction and the upstream magnetic field θ_{Bn} is larger than 45°, the shock is quasi-perpendicular; when the θ_{Bn} is less than 45°, the shock is quasi-parallel. At the quasi-parallel shock, the reflected and back streaming particles can travel far upstream along the magnetic field lines, and these particles can interact with the incident particles from the upstream solar wind, leading to the ion beam instabilities and the excitation of oblique-propagated ultralow frequency waves (Burgess, 1989; Hao, Lembege, et al., 2016; Hao, Lu, et al., 2016; Hao et al., 2017; Scholer, 1990; Su et al., 2012; X. Y. Wang & Lin, 2003; Wu et al., 2015). Many foreshock transient phenomena, such as spontaneous hot flow anomalies (Omidi et al., 2013, 2016; Zhang et al., 2013; Zhu et al., 2021), foreshock cavitons (Blanco-Cano et al., 2011, 2009; Kajdič et al., 2013; Lin, 2003; Lin & Wang, 2005; Omidi et al., 2016; M. Wang et al., 2020), and foreshock bubbles (B. Wang et al., 2020; C.-P. Wang et al., 2021) have been widely studied.

High-speed jets (HSJs), with a localized enhancement in the dynamic pressure, have been frequently observed in the quasi-parallel magnetosheath. Němeček et al. (1998) first reported the HSJs, but they referred the HSJs to as transient ion flux enhancements. In the HSJs, the dynamic pressure is enhanced and the velocity is often greater than the local Alfvén velocity, but the plasma temperature is reduced and is more isotropic than that in the surroundings (e.g., Archer & Horbury, 2013; Archer et al., 2012; Hietala et al., 2009; Karimabadi et al., 2014; Palmroth et al., 2018, 2021; Plaschke et al., 2013; Savin et al., 2008). Moreover, Archer and Horbury (2013) show that HSJs can have both increased and decreased magnetic fields, and the HSJs with increased magnetic fields are associated with a 40% increase in density.

The early event studies showed that the typical parallel scale size (parallel to the propagation direction) of the HSJs is about 1 R_E (Archer et al., 2012; Němeček et al., 1998), and the typical perpendicular size (perpendicular

to the propagation direction) of the HSJs is about a few R_E (Hietala et al., 2012). The statistical studies by Plaschke et al. (2016) showed that the characteristic parallel (perpendicular) scale size of HSJs is 0.71 R_E (1.34 R_E). Using local hybrid simulations, Hao, Lembege, et al. (2016) showed that the parallel (perpendicular) scale size of HSJs is about 1 R_E (0.2 R_E). By performing global hybrid simulations, Omidi et al. (2016) found a similar result: the parallel (perpendicular) scale size of HSJs is about 0.2–1.2 R_E (0.2–0.8 R_E). Moreover, Palmroth et al. (2018) performed a 2-D global Vlasov-hybrid simulation and found that the maximum scale sizes of the HSJs are 2.6 R_E (0.5 R_E) in the parallel (perpendicular) direction. However, the maximum scale sizes of the HSJs in the above simulations are not consistent with the observation results, in which the parallel scale size of the large-scale HSJs can be up to 5 R_E (Gunell et al., 2014) and the perpendicular scale size of many large-scale HSJs is greater than 1 R_E (Hietala et al., 2012; Plaschke et al., 2016). The formation of the large-scale HSJs is still not adequately explained.

In this study, we present 2-D global hybrid simulations to show the HSJs in Earth's quasi-parallel magnetosheath. We find some elongated HSJs formed at the quasi-parallel bow shock extend toward the quasi-perpendicular magnetosheath along with the background magnetosheath flow. The HSJs can meander because of the Kelvin-Helmholtz (K-H) instability at them. When the IMF is aligned to the solar wind velocity, the large-scale HSJs are formed at the magnetosheath where the θ_{Bn} is approaching zero. Then, some HSJs converge, leading to the formation of even larger HSJs.

2. Simulation Model

A two-dimensional global hybrid simulation model is used in this paper to study the HSJs in Earth's magnetosheath downstream of a quasi-parallel shock. In hybrid simulations, ions are treated as particles, while electrons are considered as a massless fluid. Quasi charge neutrality is assumed. The electron fluid is assumed to be isothermal in our hybrid simulation model. More details of the model can be referred to Lin and Wang (2005). A polar coordinate system (r,θ) is employed in the simulation model, and the simulation domain is limited to the noon-meridian plane of the dayside region with a range of geocentric distance 3 $R_E \leq r \leq 27$ R_E (where R_E is the Earth's radius) and polar angle $0° < \theta < 180°$. For convenience, the simulation results are represented in the Geocentric Solar Magnetospheric coordinate system. The Earth is located at the origin ($r = 0$). Solar wind inflow boundary conditions are applied for the outer boundary at $r = 27$ R_E, and outflow boundary conditions are utilized at the tailward boundary at $x = 0$. Perfect conducting boundary conditions are used at $r = 3$ R_E, and the inner magnetosphere with $r < 7$ R_E is dominated by a cold ion fluid.

Initially, the uniform solar wind ($r > 10$ R_E) and the Earth's dipole magnetic field ($r < 10$ R_E) are set in the simulation domain. The bow shock, magnetosheath, and magnetopause are formed self-consistently. The magnetic field B_0 and density N_0 in the solar wind are used to normalize the corresponding values in the simulation results. The time and length are normalized by the inverse of ion gyrofrequency ($\Omega_{i0}^{-1} = m_i/eB_0$, m_i is the ion mass) and ion inertial length $d_{i0} = c/\omega_{pi0}$ (where $\omega_{pi0} = (N_0e^2/m_i\varepsilon_0)^{1/2}$ is ion plasma frequency), respectively. The velocity is scaled to the Alfvén speed ($V_{A0} = B_0/\sqrt{\mu_0 m_i N_0}$) in the solar wind. Thus, the temperature and dynamic pressure are expressed by $T = m_i V_{A0}^2$ and $P_d = N_0 V_{A0}^2$, respectively. The ion and electron plasma beta values in the solar wind are $\beta_i = \beta_e = 0.5$. There are about 100 particles in each grid cell, and the time step is $\Delta t = 0.02\Omega_{i0}^{-1}$. In the simulation, the radius of the Earth is selected as $50d_{i0}$ (corresponding to $d_{i0} = 0.02$ R_E), which is about the realistic scale length. Total grids of $N_r \times N_\theta = 1300 \times 1400$ are used in the simulation. To produce a higher grid resolution near the magnetosheath, the grids in the r-direction are nonuniform, with a smaller grid size of $\Delta r \approx 0.5d_{i0}$ in the region of 8 $R_E \leq r \leq 14$ R_E. We present two cases in this study:

In Case 1, the radial IMF is $\boldsymbol{B_0} = (B_{x0}, B_{y0}, B_{z0}) = (1, 0, 0)B_0$, that is, the cone angle of IMF is 0° and the solar wind velocity $U_{SW} = (U_{SWx}, U_{SWy}, U_{SWz}) = (-8, 0, 0)V_{A0}$ is along the -x direction.

In Case 2, the IMF is $(0.94, 0, 0.34)$ B_0, that is, the cone angle of IMF is 20° and the solar wind velocity $(-8.5, 0, 0)V_{A0}$ is also along the -x direction. At the parallel shock ($\theta_{Bn} \approx 0$), the solar wind velocity along the bow shock normal is about 8 M_A.
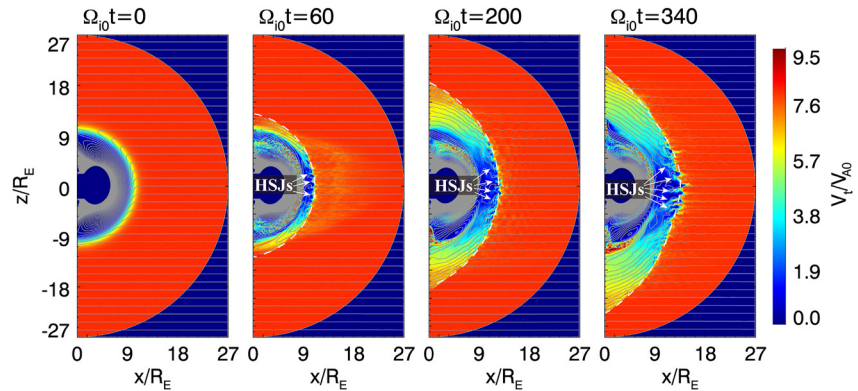
Figure 1. Contour of total ion velocity $V_t = \sqrt{V_x^2 + V_z^2}$ in the noon-midnight meridian plane obtained from Case 1 at $\Omega_{i0}t = 0$, 60, 200, and 340. The magnetic field lines are superposed in this figure with the gray lines. The white dashed lines represent the positions of the bow shock. The high-speed jet formed (at $\Omega_{i0}t = 60$, 200, and 340) at the quasi-parallel shock is marked by white arrows.

3. Simulation Results

3.1. High-Speed Jets (HSJs) Downstream of the Quasi-Parallel Shock

With an IMF cone angle of 0°, the quasi-parallel shock is formed around the subsolar region. Figure 1 shows the total velocity V_t and magnetic field lines in the noon-midnight meridian plane at $\Omega_{i0}t = 0$, 60, 200, and 340. Upstream of the quasi-parallel shock, there are low-frequency waves that are excited by the reflected ions from the shock (Burgess, 1989; Hao, Lembege, et al., 2016; Hao, Lu, et al., 2016; Liu et al., 2019; Lu et al., 2019; Wu et al., 2015). At $\Omega_{i0}t = 60$, about 10 small HSJs with a parallel scale size (parallel to the propagation direction) of less than 1 R_E are formed in the quasi-parallel magnetosheath. Then, the HSJs grow larger. At $\Omega_{i0}t = 340$, there are about 20 obvious HSJs in the meridian plane and the parallel scale size of many HSJs is larger than 1 R_E.

We first pay attention to the properties of the HSJs. Figure 2 plots the dynamic pressure P_d, total velocity V_t, ion velocity in the x-direction V_x, ion density N_i, total magnetic field B_t, and temperatures T at $\Omega_{i0}t = 340$. In the HSJs, besides the obvious velocity enhancement, the plasma density and magnetic field are also enhanced, while the temperature is low (e.g., Archer et al., 2012; Hietala et al., 2009; Karimabadi et al., 2014; Palmroth et al., 2018, 2021; Savin et al., 2008). Six large-scale HSJs near the subsolar point (where θ_{Bn} is approaching zero) are marked by the white arrows in Figure 2, and the scale sizes of these HSJs are about 1.1–2.5 R_E in the parallel direction and about 0.2–0.5 R_E in the perpendicular direction. In Figure 2, magnetosheath cavities (MCs) (denoted with the red arrows) are formed between large-scale HSJs. In contrast to the HSJs, the velocity, density, and magnetic field are lower than those in the surroundings, and the temperature has an obvious enhancement in the MCs (Katırcıoğlu et al., 2009; Omidi et al., 2016). Moreover, in Figure 2c, there are sunward flows (about 1.5 V_A) in the MCs and they are also shown in previous observations (Plaschke et al., 2017; Shue et al., 2009) and simulations (Karimabadi et al., 2014).

Figure 3 plots the evolution of HSJs in the high-latitude magnetosheath (i.e., the flank magnetosheath). The HSJs identified to possess a dynamic pressure two times the background magnetosheath value (violet contour) are smaller than those near the subsolar point. In the high-latitude magnetosheath, the magnetic field is nearly parallel to the magnetosheath flow around the magnetopause (see Figure 1). Thus, the HSJs formed at the quasi-parallel bow shock extend over a long distance and toward the quasi-perpendicular magnetosheath along the magnetic field and the background flows but the dynamic pressure in them gradually decreases. In Figure 3, the HSJs identified to possess a dynamic pressure 1.5 times the background magnetosheath value are denoted by the black contour and these weak HSJs are elongated. In the elongated HSJs, the total velocity and ion density are enhanced and temperature is decreased (Figure 4). However, the magnetic field in the elongated HSJs (away from the bow shock) is not always increased, which is different from the HSJs near the bow shock (Figure 4c). As the elongated HSJs move in the magnetosheath, filamentary structures of the velocity, ion density, and temperature occur in the magnetosheath. The filamentary structures are the traces of HSJs moving in the magnetosheath and they can be up to 15 R_E long and about 0.1–0.2 R_E wide. Moreover, filamentary structures are also formed by the HSJs near
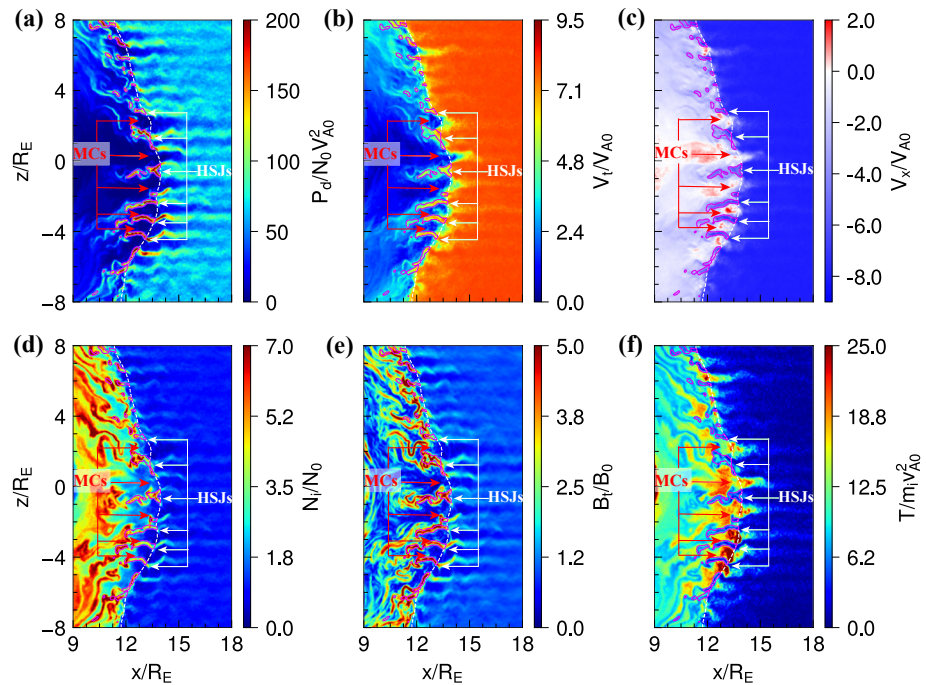
Figure 2. Contours of (a) dynamic pressure P_d (b) total ion velocity V_t, (c) ion velocity in the x-direction V_x, (d) ion density N_i, (e) total magnetic field B_t, and (f) ion temperature T in the noon-midnight meridian plane at $\Omega_{i0}t = 340$. The violet contour represents the dynamic pressure that is two times the background dynamic pressure in the magnetosheath, as defined in Archer and Horbury (2013). The white dashed lines represent the positions of the bow shock. The high-speed jets and magnetosheath cavities formed near the subsolar point are marked by white and red arrows, respectively.
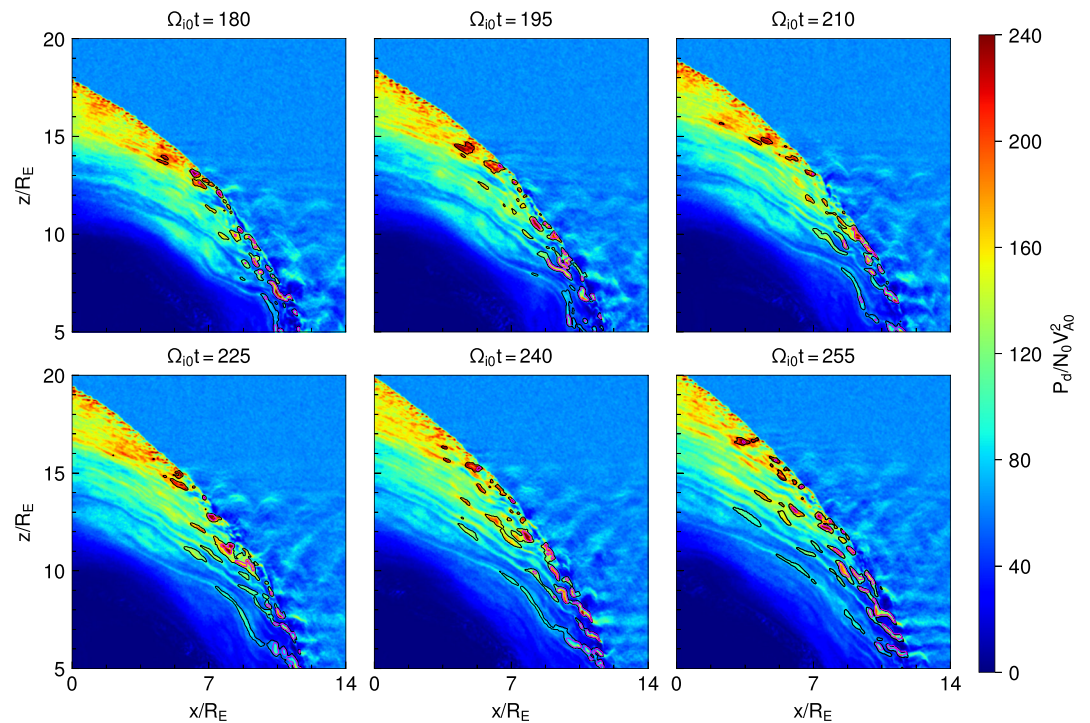

Figure 3. Contour of dynamic pressure P_d in the noon-midnight meridian plane at $\Omega_{i0}t = 180, 195, 210, 225, 240$, and 255. The violet (black) contour represents the dynamic pressure that is two (1.5) times the background dynamic pressure in the magnetosheath.

Figure 4. Contours of (a) total velocity V_t, (b) ion density N_i, (c) total magnetic field B_t, and (d) ion temperature T obtained from Case 1 at $\Omega_{i0}t = 255$. The violet (black) contour represents the dynamic pressure that is two (1.5) times the background dynamic pressure in the magnetosheath.
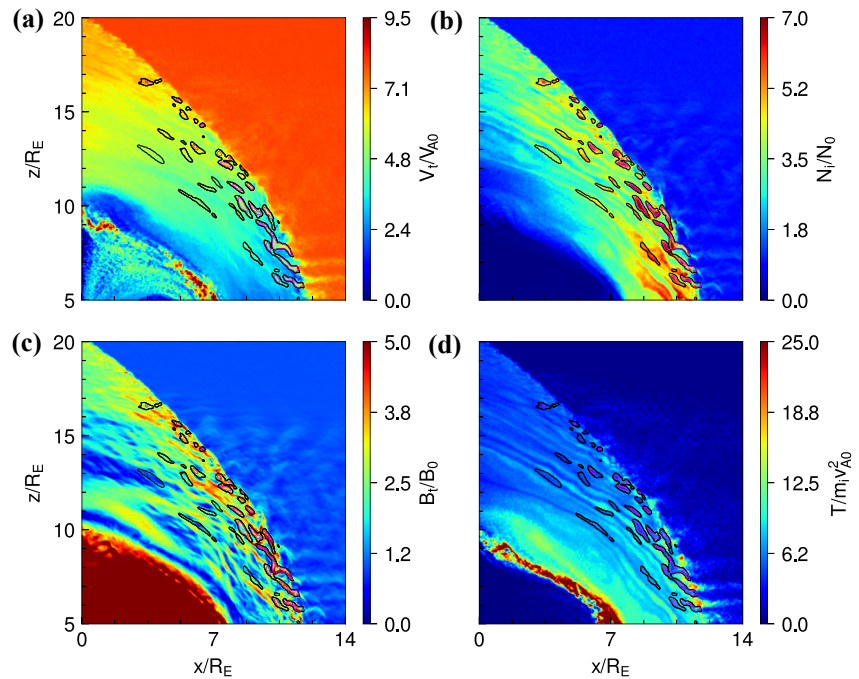
the subsolar point (see Figure 2) but they are shorter than those in the high-latitude magnetosheath because of obstructions of the magnetopause.

3.2. Kelvin-Helmholtz Instability at HSJs

After the HSJs are formed, some of them become larger and begin to meander. Figure 5 shows the magnetic field lines, total velocity V_t, and local Alfvén velocity V_{AL} at $\Omega_{i0}t = 410$, 430, 450, and 470. Total velocity and local Alfvén velocity are significantly increased in the HSJs. At $\Omega_{i0}t = 410$ (Figure 5a), the HSJ marked by a white arrow is relatively straight in the x-direction and the magnetic field lines in the HSJ have little curvature. Then, at $\Omega_{i0}t = 430$–470, the HSJ becomes more and more meandering and the curvature of the magnetic field lines in the HSJ also increases.

To study what causes the meandering of the HSJs, we examine the K-H instability for a representative HSJ (marked by a white arrow in Figure 5). Figure 6 plots the spatial profiles of total velocity V_t and local Alfvén
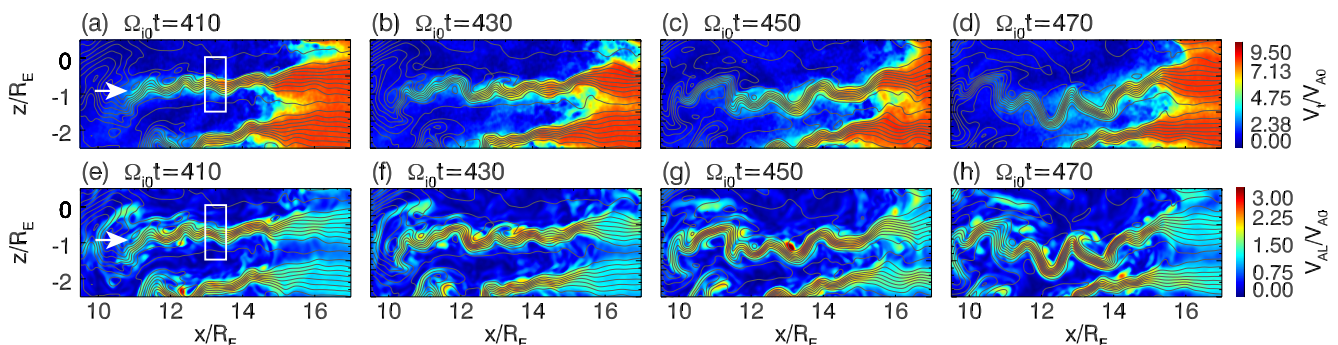

Figure 5. Contours of (a–d) total ion velocity V_t and (e–h) local Alfvén velocity V_{AL} obtained from Case 1 at $\Omega_{i0}t = 410$, 430, 450, and 470. The white arrow represents the meandered High-speed jet caused by the Kelvin-Helmholtz instability. The magnetic field lines are superposed in this figure with the gray lines.
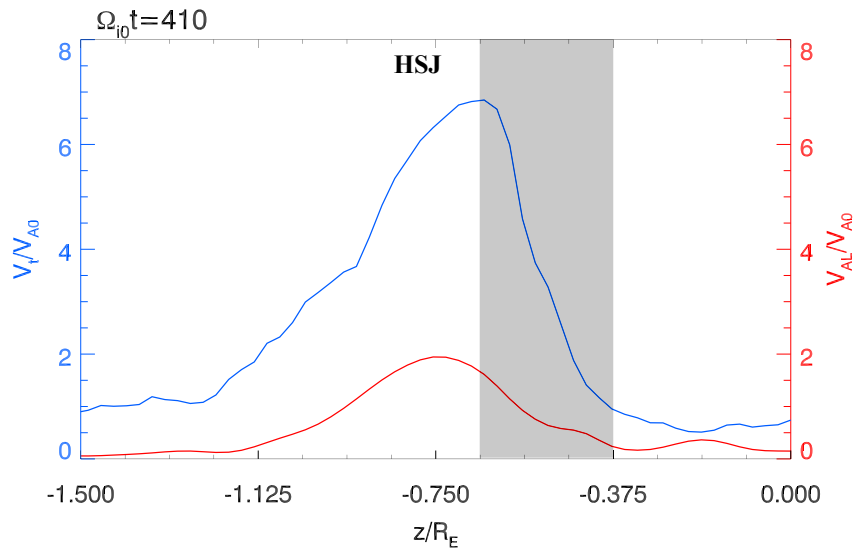
Figure 6. Spatial profiles of the total velocity V_t and local Alfvén velocity V_{AL} as a function of z, averaged within 12.987 $R_E < x < 13.500\ R_E$, which is denoted by the white box in Figures 5a and 5e. The gray region is the velocity jump in the High-speed jet (HSJ).

velocity V_{AL} as a function of z, averaged within 12.987 $R_E < x < 13.5\ R_E$, which is denoted by the white box in Figures 5 and 5e.

In Figure 5, the plasma velocity in HSJs is basically aligned to the magnetic field lines, that is, $\mathbf{k} \parallel \mathbf{V}_{HSJ} \parallel \mathbf{B}_{HSJ}$ (where $\mathbf{k}$ is the wavenumber along the x-direction, V_{HSJ} is the maximum velocity in the HSJ, and B_{HSJ} is the magnetic field in the HSJ). In principle, the fastest growth rate of the K-H instability occurs when $\mathbf{k}$ is perpendicular to the magnetic field because this way the instability is not stabilized by the magnetic tension force. Nevertheless, Miura and Pritchett (1982) showed that the K-H instability can still grow when the velocity is aligned to the magnetic field, according to which the unstable condition is $M_s^2 < 4$ and $M_A^2 > 4$, where $M_s = V_0/c_s$, $V_0 = V_{HSJ} - V_{MC}$ is the total velocity jump, V_{MC} is the velocity in MCs, c_s is the sound speed, $M_A = V_0/V_{AL\_HSJ}$, and $V_{AL\_HSJ} = 2V_{A0}$ is the local Alfvén velocity in the HSJ (see Figures 5 and 6). For a representative HSJ, $V_0 = 7V_{A0}$ (gray region in Figure 6) and $c_s = 6.93V_{A0}$ ($T_i \approx 16\ m_i V_{A0}^2$), so $M_s^2 = 1 < 4$ and $M_A^2 = 12.25 > 4$, and the K-H instability can therefore be excited at the HSJs.

In our study, for the representative HSJ, $M_A^{-1} = 0.29$, which yields a maximum growth rate at $2ka \approx 0.7$ according to Figure 4 in Miura and Pritchett (1982). For the representative HSJ, the wavelength λ is about 2 R_E (see Figure 5d) and the shear length $2a$ (the perpendicular scale size of the HSJ) is about 0.3 R_E (see Figure 6). Therefore, the result is $2ka \approx 0.9$, which is in good agreement with the theoretical results. The above examination shows that the K-H instability can grow and is responsible for the meandering of the HSJs in our simulations. Note that the K-H instability does not break the HSJs, which is possibly because the magnetic field aligned to the velocity inhibits the further development of the instability.

The K-H instability is more likely to occur in the HSJs between two MCs because the velocity jump is large. In the high-latitude magnetosheath, there are no MCs and the background magnetosheath velocity is large. Therefore, the velocity jump between the HSJs and the background magnetosheath is small (Figures 1 and 4a) and the K-H instability cannot occur there.

3.3. What Controls the Formation of Large-Scale HSJs?

To study how the large-scale HSJs are formed, we perform another case and compare it with Case 1. In Case 2, the IMF cone angle is 20° and the solar wind velocity is $8.5M_A$ along the $-x$ direction. At the parallel shock ($\theta_{Bn} \approx 0$), the solar wind velocity along the bow shock normal is about $8M_A$, which is similar to Case 1. Figure 7 shows the total velocity V_t and magnetic field lines obtained from Case 2 at $\Omega_{i0}t = 0$, 60, 200, and 340. The quasi-parallel shock is mainly located in the Northern Hemisphere, and the quasi-perpendicular shock is located in the Southern
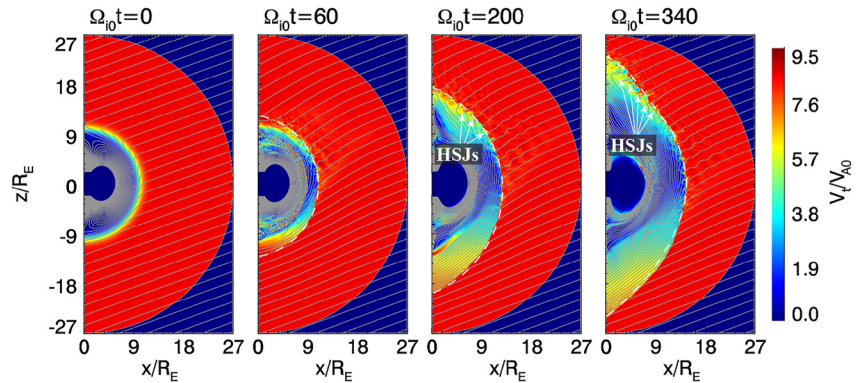
Figure 7. Contour of total ion velocity V_t at $\Omega_{i0}t = 0$, 60, 200, and 340 obtained from Case 2 (interplanetary magnetic field cone angle is 20° and the solar wind is along the $-x$ direction). The magnetic field lines are superposed in this figure with the gray lines. The white dashed lines represent positions of the bow shock. Some high-speed jets are marked by white arrows.

Hemisphere. At $\Omega_{i0}t = 200$ and 340, many HSJs are formed in the quasi-parallel magnetosheath. Figure 8 plots the dynamic pressure P_d, total velocity V_t, ion velocity in the x-direction V_x, ion density N_i, total magnetic field B_t, and temperature T obtained from Case 2 at $\Omega_{i0}t = 340$. In Figure 8, the HSJs have a parallel (perpendicular) scale size of about 0.3–1.4 R_E (0.1–0.3 R_E) and they are smaller than those in Case 1 (Figure 2). Similar to Case 1, besides the obvious velocity enhancement, the plasma density and magnetic field are also enhanced, while the temperature is low. However, in Figure 8, the MCs are small than that in Case 1 and the sunward flows in the MCs are missing. The filamentary structures are also formed by the HSJs but are shorter than those in Case 1.
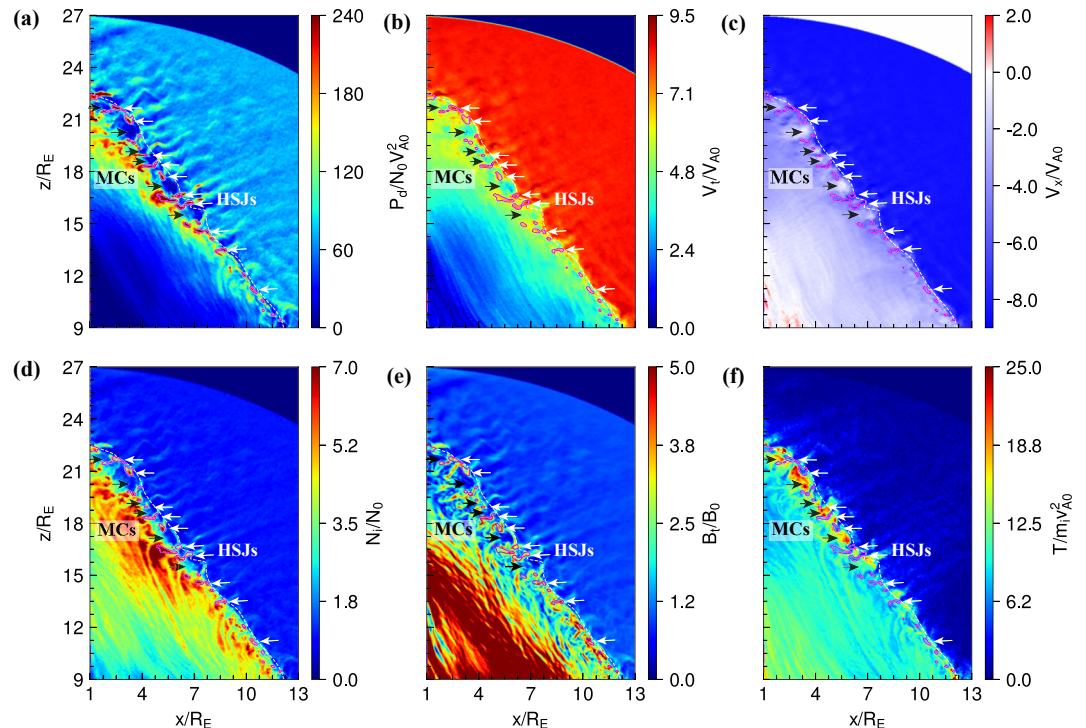
Figure 8. Contours of (a) dynamic pressure P_d, (b) total ion velocity V_t, (c) ion velocity in the x-direction V_x, (d) ion density N_i, (e) total magnetic field B_t, and (f) ion temperature T obtained from Case 2 at $\Omega_{i0}t = 340$. The violet contour represents the dynamic pressure that is two times the background dynamic pressure in the magnetosheath. The white dashed lines represent positions of the bow shock. Some high-speed jets and magnetosheath cavities are marked by white and black arrows, respectively.
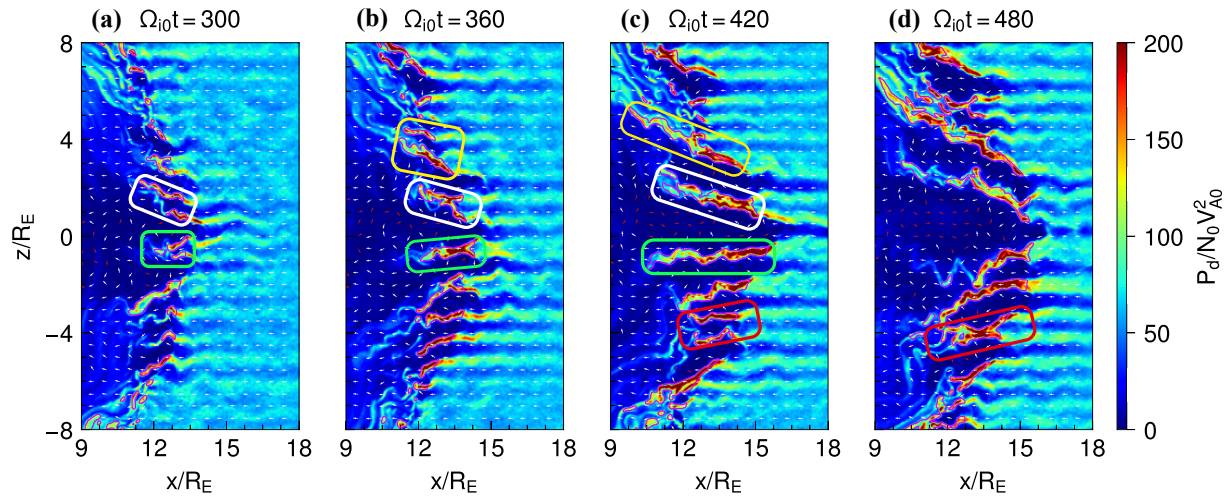
Figure 9. (a–d) Contour of dynamic pressure P_d obtained from Case 1 at $\Omega_{i0}t$ = 300, 360, 420, and 480. The violet contour represents the dynamic pressure that is two times the background dynamic pressure in the magnetosheath. Some high-speed jets (HSJs) formed near the subsolar point are marked by white, green, yellow, and red boxes. The large regions with low velocity (between the large-scale HSJs) are the magnetosheath cavities, which are also shown in Figure 2. The arrows represent the direction of plasma flows. White arrows denote the flows with $V_{ix} < 0$ and red arrows denote the flows with $V_{ix} > 0$.

Figure 9 shows the evolution of the HSJs (Case 1) near the subsolar point at $\Omega_{i0}t$ = 300–480. There are vortexes represented by arrows in the large MCs. In Figure 9a, at $\Omega_{i0}t$ = 300, two HSJs exist in the white box and their scale sizes are about 1–2 R_E in the parallel direction and about 0.2 R_E in the perpendicular direction. Then, the HSJs in the white box get very close due to the push of two vortexes beside the HSJs at $\Omega_{i0}t$ = 360 and they converge to form a larger one at $\Omega_{i0}t$ = 420. The scale sizes of the large-scale HSJ in the white box (Figure 9c) are about 4.5 R_E in the parallel direction and 0.6 R_E in the perpendicular direction. Similarly, two HSJs in the green box converge to form a larger one (about 5 R_E in parallel and 0.4 R_E in perpendicular) from $\Omega_{i0}t$ = 300 to $\Omega_{i0}t$ = 420; two HSJs in the red box converge to form a larger one from $\Omega_{i0}t$ = 420 to $\Omega_{i0}t$ = 480; and two HSJs in the yellow box converge to form one from $\Omega_{i0}t$ = 360 to $\Omega_{i0}t$ = 420. The convergence of several HSJs is further conducive to the formation of the larger HSJs both in the parallel and perpendicular directions. The low-velocity regions between the HSJs are MCs that are also shown in Figure 2. With the convergence of the HSJs, the MCs are getting larger.

4. Conclusions and Discussion

Based on our 2-D global hybrid simulation results, the main conclusions are summarized as follows.

1. When the quasi-parallel shock forms near the subsolar point, many HSJs with an obvious dynamic pressure enhancement begin to form in the quasi-parallel magnetosheath. In the HSJs, the plasma velocity, density, and magnetic field are enhanced but the temperature is lowered.
2. Along with the background magnetosheath flow, many elongated HSJs formed at the quasi-parallel bow shock extend toward the quasi-perpendicular magnetosheath. As the elongated HSJs move in the magnetosheath, filamentary structures of the velocity, ion density, and temperature occur in the magnetosheath. The filamentary structures are the traces of HSJs moving in the magnetosheath.
3. The K-H instability is more likely to be excited in the HSJs between two MCs with a rapid growth rate, which causes meandering of the HSJs.
4. The alignment between the IMF and the solar wind velocity favors the formation of large-scale HSJs with a parallel scale size of about 2.5 R_E. Several of these HSJs can converge and form even larger HSJs with a parallel (perpendicular) scale size of 5 R_E (0.6 R_E). Sunward flows (with a speed of $\sim 1.5V_A$) are found between two large-scale HSJs when the IMF is aligned to the solar wind velocity.

Many observational studies showed that the HSJs are associated with the earthward motion of the magnetopause (Amata et al., 2011; Archer et al., 2012; Hietala et al., 2009, 2012; Plaschke et al., 2016; Shue et al., 2009), and the indented magnetopause perturbations can propagate into the magnetosphere, leading to localized and short-lived enhanced convection flow channels (Hietala et al., 2012). Moreover, the HSJs may trigger

the magnetopause reconnection (Hietala et al., 2018; Nykyri et al., 2019) and form throat aurora in the ionosphere (Han et al., 2017, 2019). The scale size of HSJs determine how many particles and how much energy from the solar wind they can carry, and the large-scale HSJs have a greater impact on Earth's magnetosphere (Plaschke et al., 2016). In this study, we find that two factors control the formation of large-scale HSJs, one is the angle between the IMF and the solar wind velocity and the other is the convergence of several HSJs. When the IMF is aligned to the solar wind velocity, the large-scale HSJs can be formed at the quasi-parallel magnetosheath where θ_{Bn} is approaching zero. The angle between the IMF and solar wind velocity may have a significant impact on the interaction between short, large-amplitude magnetic structures and shock front, which determines the scale size of HSJs. It deserves further study. Furthermore, several HSJs are closed due to the vortexes in two MCs and they converge to form an even larger HSJ. The scale size of the large-scale HSJs in this study are consistent with that in observations (Gunell et al., 2014; Hietala et al., 2012; Nykyri et al., 2019; Plaschke et al., 2016). Although some previous global hybrid simulations (including 2-D and 3-D) have studied the formation and evolution of HSJs (Ng et al., 2021; Omelchenko et al., 2021; Palmroth et al., 2018, 2021), the large-scale HSJs are not found because the IMF is not aligned to the solar wind velocity. Moreover, deducing the scale size of the Earth and the low-resolution of simulations prevent some simulations from studying the convergence of the HSJs (Karimabadi et al., 2014; Omelchenko et al., 2021). The convergence of the HSJs may be a common phenomenon in the magnetosheath and deserves further studies by using spacecraft observations and realistic-scale 3-D global simulations. With the development of computing resources, we will have the opportunity to perform a realistic-scale 3D global simulation, and we predict that the HSJs will easily converge in the realistic-scale magnetosheath, not just in the z-direction.

In this study, the maximum perpendicular scale size of the large HSJs is about $1R_E$. However, by analyzing the statistical observation of HSJs, Plaschke et al. (2016) show the characteristic perpendicular scale size is 1.34 R_E. The reason for this contradiction with Plaschke et al. (2016) may be because the HSJs are not columnar in the actual three-dimensional nature. Omelchenko et al. (2021) performed a three-dimensional global hybrid simulation of a reduced Earth and showed that the HSJs are pancake-like dynamic pressure structures with two different perpendicular scale sizes: one is along the dawn-dusk direction (6 R_E) and the other is in the noon-meridian plane (0.6 R_E). The scale size of HSJs in the noon-meridian plane obtained from Omelchenko et al. (2021) is consistent with our results. However, to study the scale size of HSJs in 3-D nature still requires a realistic-scale 3D global simulation.

Filamentary structures of the magnetic field, ion density, and temperature have been observed in the magnetosheath (Cai & Wei, 2020). Using 2-D global hybrid simulations, Lin (2003) found that filamentary structures with in-phase magnetic field and density perturbations are formed from evolution of diamagnetic cavities in the foreshock regions, which extend through the shock transition and follow the streamlines into the magnetosheath. These field-aligned elongated structures were suggested to be due to the ion beam-plasma instability (Lin & Wang, 2005; X. Y. Wang & Lin, 2006). Omidi et al. (2014) suggested that the magnetosheath filamentary structures are formed by the shock accelerated ions. In this study, based on a high-resolution global hybrid simulation with a realistic d_{i0}, we find the magnetosheath filamentary structures are formed by the elongated HSJs with a large parallel but small perpendicular scale size and they have phase relations among magnetic field, velocity, density, and temperature similar to Lin (2003) and Lin and Wang (2005). Since the magnetosheath magnetic field is nearly parallel to the magnetosheath flow around the magnetopause (see Figure 1), the HSJs extend over a long distance along the magnetic field and the magnetosheath flow. Therefore, the traces of HSJs moving in the magnetosheath are the filamentary structures. Recently, HSJs are also found in the magnetosheath downstream of the quasi-perpendicular shock and they are thought to be derived from magnetic flux tubes connected to the quasi-parallel bow shock (Kajdič et al., 2021). In this study, the elongated HSJs as flux tubes transfer particles and energy from the solar wind toward the quasi-perpendicular magnetosheath, which can help understand the formation of quasi-perpendicular magnetosheath HSJs.

A detailed examination indicates that the K-H instability can be excited in many HSJs with a rapid growth rate, resulting in the meandering of HSJs in their parallel propagated direction. However, the K-H instability does not break the HSJs because the strong magnetic field can inhibit further development of the instability. With Cluster observations, many current sheets, as well as magnetic reconnection, were observed by Retinò et al. (2007) in the turbulent magnetosheath downstream of a quasi-parallel shock. The K-H instability can distort the magnetic field

lines at HSJs to form current sheets in the magnetosheath. The effects of HSJs on the formation of current sheets and the magnetosheath reconnection will be studied in future work.

Data Availability Statement

The authors gratefully acknowledge the data resources from the "National Space Science Data Center, National Science & Technology Infrastructure of China (http://www.nssdc.ac.cn)." In this study, the simulation data that are used to plot the figures can be downloaded from https://dx.doi.org/10.12176/01.99.02320.

References

Amata, E., Savin, S. P., Ambrosino, D., Bogdanova, Y. V., Marcucci, M. F., Romanov, S., & Skalsky, A. (2011). High kinetic energy density jets in the Earth's magnetosheath: A case study. *Planetary and Space Science*, *59*(7), 482–494. https://doi.org/10.1016/j.pss.2010.07.021

Archer, M. O., & Horbury, T. S. (2013). Magnetosheath dynamic pressure enhancements: Occurrence and typical properties. *Annales Geophysicae*, *31*(2), 319–331. https://doi.org/10.5194/angeo-31-319-2013

Archer, M. O., Horbury, T. S., & Eastwood, J. P. (2012). Magnetosheath pressure pulses: Generation downstream of the bow shock from solar wind discontinuities. *Journal of Geophysical Research*, *117*(A5), A05228. https://doi.org/10.1029/2011JA017468

Blanco-Cano, X., Kajdič, P., Omidi, N., & Russell, C. T. (2011). Foreshock cavitons for different interplanetary magnetic field geometries: Simulations and observations. *Journal of Geophysical Research*, *116*(A9), A09101. https://doi.org/10.1029/2010JA016413

Blanco-Cano, X., Omidi, N., & Russell, C. T. (2009). Global hybrid simulations: Foreshock waves and cavitons under radial interplanetary magnetic field geometry. *Journal of Geophysical Research*, *114*(A1), A01216. https://doi.org/10.1029/2008JA013406

Burgess, D. (1989). Cyclic behavior at quasi-parallel collisionless shocks. *Geophysical Research Letters*, *16*(5), 345–348. https://doi.org/10.1029/GL016i005p00345

Cai, C., & Wei, X. (2020). Multipoint observations of magnetosheath response to foreshock transients. *Journal of Geophysical Research: Space Physics*, *125*, e2019JA027416. https://doi.org/10.1029/2019JA027416

Fairfield, D. H. (1971). Average and unusual locations of the Earth's magnetopause and bow shock. *Journal of Geophysical Research*, *76*(28), 6700–6716. https://doi.org/10.1029/JA076i028p06700

Gunell, H., Stenberg Wieser, G., Mella, M., Maggiolo, R., Nilsson, H., Darrouzet, F., et al. (2014). Waves in high-speed plasmoids in the magnetosheath and at the magnetopause. *Annales Geophysicae*, *32*(8), 991–1009. https://doi.org/10.5194/angeo-32-991-2014

Han, D.-S., Hietala, H., Chen, X.-C., Nishimura, Y., Lyons, L. R., Liu, J.-J., et al. (2017). Observational properties of dayside throat aurora and implications on the possible generation mechanisms. *Journal of Geophysical Research: Space Physics*, *122*, 1853–1870. https://doi.org/10.1002/2016JA023394

Han, D.-S., Xu, T., Jin, Y., Oksavik, K., Chen, X.-C., Liu, J.-J., et al. (2019). Observational evidence for throat aurora being associated with magnetopause reconnection. *Geophysical Research Letters*, *46*, 7113–7120. https://doi.org/10.1029/2019GL083593

Hao, Y., Gao, X., Lu, Q., Huang, C., Wang, R., & Wang, S. (2017). Reformation of rippled quasi-parallel shocks: 2-D hybrid simulations. *Journal of Geophysical Research: Space Physics*, *122*, 6385–6396. https://doi.org/10.1002/2017JA024234

Hao, Y., Lembege, B., Lu, Q. M., & Guo, F. (2016). Formation of downstream high-speed jets by a rippled nonstationary quasi-parallel shock: 2-D hybrid simulations. *Journal of Geophysical Research: Space Physics*, *121*, 2080–2094. https://doi.org/10.1002/2015JA021419

Hao, Y., Lu, Q. M., Gao, X. L., & Wang, S. (2016). Ion dynamics at a rippled quasi-parallel shock: 2D hybrid simulations. *The Astrophysical Journal*, *823*, 7. https://doi.org/10.3847/0004-637X/823/1/7

Hietala, H., Laitinen, T. V., Andreeova, K., Vainio, R., Vaivads, A., Palmroth, M., et al. (2009). Supermagnetosonic jets behind a collisionless quasi-parallel shock. *Physical Review Letters*, *103*, 245001. https://doi.org/10.1103/PhysRevLett.103.245001

Hietala, H., Partamies, N., Laitinen, T. V., Clausen, L. B. N., Facskó, G., Vaivads, A., et al. (2012). Supermagnetosonic subsolar magnetosheath jets and their effects: From the solar wind to the ionospheric convection. *Annales Geophysicae*, *30*(1), 33–48. https://doi.org/10.5194/angeo-30-33-2012

Hietala, H., Phan, T. D., Angelopoulos, V., Oieroset, M., Archer, M. O., Karlsson, T., & Plaschke, F. (2018). In situ observations of a magnetosheath high-speed jet triggering magnetopause reconnection. *Geophysical Research Letters*, *45*(4), 1732–1740. https://doi.org/10.1002/2017GL076525

Kajdič, P., Blanco-Cano, X., Omidi, N., Meziane, K., Russell, C. T., Sauvaud, J. A., et al. (2013). Statistical study of foreshock cavitons. *Annales Geophysicae*, *31*(12), 2163–2178. https://doi.org/10.5194/angeo-31-2163-2013

Kajdič, P., Raptis, S., Blanco-Cano, X., & Karlsson, T. (2021). Causes of jets in the quasi-perpendicular magnetosheath. *Geophysical Research Letters*, *48*, e2021GL093173. https://doi.org/10.1029/2021GL093173

Karimabadi, H., Roytershteyn, V., Vu, H. X., Omelchenko, Y. A., Scudder, J., Daughton, W., et al. (2014). The link between shocks, turbulence, and magnetic reconnection in collisionless plasmas. *Physics of Plasmas*, *21*(6), 062308. https://doi.org/10.1063/1.4882875

Katırcıoğlu, F. T., Kaymaz, Z., Sibeck, D. G., & Dandouras, I. (2009). Magnetosheath cavities: Case studies using cluster observations. *Annales Geophysicae*, *27*(10), 3765–3780. https://doi.org/10.5194/angeo-27-3765-2009

Lin, Y. (2003). Global-scale simulation of foreshock structures at the quasi-parallel bow shock. *Journal of Geophysical Research*, *108*(A11), 1390. https://doi.org/10.1029/2003JA009991

Lin, Y., & Wang, X. Y. (2005). Three-dimensional global hybrid simulation of dayside dynamics associated with the quasi-parallel bow shock. *Journal of Geophysical Research*, *110*(A12), A12216. https://doi.org/10.1029/2005JA011243

Liu, T. Z., Hietala, H., Angelopoulos, V., Omelchenko, Y., Roytershteyn, V., & Vainio, R. (2019). THEMIS observations of particle acceleration by a magnetosheath jet-driven bow wave. *Geophysical Research Letters*, *46*, 7929–7936. https://doi.org/10.1029/2019GL082614

Lu, Q., Wang, H., Wang, X., Lu, S., Wang, R., Gao, X., & Wang, S. (2019). Turbulence-driven magnetic reconnection in the magnetosheath downstream of a quasi-parallel shock: A three-dimensional global hybrid simulation. *Geophysical Research Letters*, *47*, e2019GL085661. https://doi.org/10.1029/2019GL085661

Miura, A., & Pritchett, P. L. (1982). Nonlocal stability analysis of the MHD Kelvin-Helmholtz instability in a compressible plasma. *Journal of Geophysical Research*, *87*(A9), 7431–7444. https://doi.org/10.1029/JA087iA09p07431

Němeček, Z., Safránková, J., Prech, L., Sibeck, D. G., Kokubun, S., & Mukai, T. (1998). Transient flux enhancements in the magnetosheath. *Geophysical Research Letters*, *25*, 1273–1276. https://doi.org/10.1029/98GL50873

Ng, J., Chen, L.-J., & Omelchenko, Y. A. (2021). Bursty magnetic reconnection at the Earth's magnetopause triggered by high-speed jets. *Physics of Plasmas*, *28*, 092902. https://doi.org/10.1063/5.0054394

Nykyri, K., Bengtson, M., Angelopoulos, V., Nishimura, Y. T., & Wing, S. (2019). Can enhanced flux loading by high-speed jets lead to a substorm? Multipoint detection of the christmas day substorm onset at 08:17 UT, 2015. *Journal of Geophysical Research: Space Physics*, *124*, 4314–4340. https://doi.org/10.1029/2018JA026357

Omelchenko, Y. A., Chen, L. J., & Ng, J. (2021). 3D space-time adaptive hybrid simulations of magnetosheath high-speed jets. *Journal of Geophysical Research: Space Physics*, *126*(7), e2020JA029035. https://doi.org/10.1029/2020JA029035

Omidi, N., Berchem, J., Sibeck, D., & Zhang, H. (2016). Impacts of spontaneous hot flow anomalies on the magnetosheath and magnetopause. *Journal of Geophysical Research: Space Physics*, *121*(4), 3155–3169. https://doi.org/10.1002/2015JA022170

Omidi, N., Sibeck, D., Gutynska, O., & Trattner, K. J. (2014). Magnetosheath filamentary structures formed by ion acceleration at the quasi-parallel bow shock. *Journal of Geophysical Research: Space Physics*, *119*, 2593–2604. https://doi.org/10.1002/2013JA019587

Omidi, N., Zhang, H., Sibeck, D., & Turner, D. (2013). Spontaneous hot flow anomalies at quasi-parallel shocks: 2. Hybrid simulations. *Journal of Geophysical Research: Space Physics*, *118*(1), 173–180. https://doi.org/10.1029/2012JA018099

Palmroth, M., Hietala, H., Plaschke, F., Archer, M., Karlsson, T., Blanco-Cano, X., et al. (2018). Magnetosheath jet properties and evolution as determined by a global hybrid-Vlasov simulation. *Annales Geophysicae*, *36*(5), 1171–1182. https://doi.org/10.5194/angeo-36-1171-2018

Palmroth, M., Raptis, S., Suni, J., Karlsson, T., Turc, L., Johlander, A., et al. (2021). Magnetosheath jet evolution as a function of lifetime: Global hybrid-Vlasov simulations compared to MMS observations. *Annales Geophysicae*, *39*(2), 289–308. https://doi.org/10.5194/angeo-39-289-2021

Peredo, M., Slavin, J. A., Mazur, E., & Curtis, S. A. (1995). Three-dimensional position and shape of the bow shock and their variation with Alfvénic, sonic and magnetosonic Mach numbers and interplanetary magnetic field orientation. *Journal of Geophysical Research*, *100*(A5), 7907–7916. https://doi.org/10.1029/94JA02545

Plaschke, F., Hietala, H., & Angelopoulos, V. (2013). Anti-sunward high-speed jets in the subsolar magnetosheath. *Annales Geophysicae*, *31*(10), 1877–1889. https://doi.org/10.5194/angeo-31-1877-2013

Plaschke, F., Hietala, H., Angelopoulos, V., & Nakamura, R. (2016). Geoeffective jets impacting the magnetopause are very common. *Journal of Geophysical Research: Space Physics*, *121*(4), 3240–3253. https://doi.org/10.1002/2016JA022534

Plaschke, F., Karlsson, T., Hietala, H., Archer, M., Vörös, Z., Nakamura, R., et al. (2017). Magnetosheath high-speed jets: Internal structure and interaction with ambient plasma. *Journal of Geophysical Research: Space Physics*, *122*(10), 10157–10175. https://doi.org/10.1002/2017JA024471

Retinò, A., Sundkvist, D., Vaivads, A., Mozer, F., André, M., & Owen, C. J. (2007). In situ evidence of magnetic reconnection in turbulent plasma. *Nature Physics*, *3*(4), 235–238. https://doi.org/10.1038/nphys574

Savin, S., Amata, E., Zelenyi, L., Budaev, V., Consolini, G., Treumann, R., et al. (2008). High energy jets in the Earth's magnetosheath: Implications for plasma dynamics and anomalous transport. *JETP Letters*, *87*(11), 593–599. https://doi.org/10.1134/S0021364008110015

Scholer, M. (1990). Diffuse ions at a quasi-parallel collisionless shock: Simulations. *Geophysical Research Letters*, *17*, 1821–1824. https://doi.org/10.1029/GL017i011p01821

Shue, J.-H., Chao, J.-K., Song, P., McFadden, J. P., Suvorova, A., Angelopoulos, V., et al. (2009). Anomalous magnetosheath flows and distorted subsolar magnetopause for radial interplanetary magnetic fields. *Geophysical Research Letters*, *36*, L18112. https://doi.org/10.1029/2009GL039842

Su, Y. Q., Lu, Q. M., Huang, C., Wu, M. Y., Gao, X. L., & Wang, S. (2012). Particle acceleration and generation of diffuse superthermal ions at a quasi-parallel collisionless shock: Hybrid simulations. *Journal of Geophysical Research*, *117*(A8), A08107. https://doi.org/10.1029/2012JA017736

Wang, B., Liu, T., Nishimura, Y., Zhang, H., Hartinger, M., Shi, X., et al. (2020). Global propagation of magnetospheric Pc5 ULF waves driven by foreshock transients. *Journal of Geophysical Research: Space Physics*, *125*, e2020JA028411. https://doi.org/10.1029/2020JA028411

Wang, C.-P., Wang, X., Liu, T. Z., & Lin, Y. (2021). A foreshock bubble driven by an IMF tangential discontinuity: 3D global hybrid simulation. *Geophysical Research Letters*, *48*, e2021GL093068. https://doi.org/10.1029/2021GL093068

Wang, M., Yao, S., Shi, Q., Zhang, H., Tian, A., Degeling, A. W., et al. (2020). Propagation properties of foreshock cavitons: Cluster observations. *Science China Technological Sciences*, *63*(1), 173–182. https://doi.org/10.1007/s11431-018-9450-3

Wang, X. Y., & Lin, Y. (2003). Generation of nonlinear Alfvén and magnetosonic waves by beam–plasma interaction. *Physics of Plasmas*, *10*(9), 3528–3538. https://doi.org/10.1063/1.1599359

Wang, X. Y., & Lin, Y. (2006). Generation of filamentary structures by beam-plasma interaction. *Physics of Plasmas*, *13*, 052102. https://doi.org/10.1063/1.2197797

Wu, M., Hao, Y., Lu, Q., Huang, C., Guo, F., & Wang, S. (2015). The role of large amplitude upstream low-frequency waves in the generation of superthermal ions at a quasi-parallel collisionless shock: Cluster observations. *The Astrophysical Journal*, *808*, 2. https://doi.org/10.1088/0004-637X/808/1/2

Zhang, H., Sibeck, D. G., Zong, Q. G., Omidi, N., Turner, D., & Clausen, L. B. N. (2013). Spontaneous hot flow anomalies at quasi-parallel shocks: 1. Observations. *Journal of Geophysical Research: Space Physics*, *118*(6), 3357–3363. https://doi.org/10.1002/jgra.50376

Zhu, X., Wang, M., Shi, Q., Zhang, H., Tian, A., Yao, S., et al. (2021). Motion of classic and spontaneous hot flow anomalies observed by Cluster. *Journal of Geophysical Research: Space Physics*, *126*, e2021JA029418. https://doi.org/10.1029/2021JA029418